The asymmetric opening of HIV-1 Env by a potent indoline CD4 mimetic enables anti-CoRBS Abs to mediate ADCC

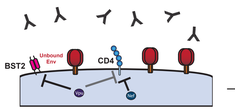
500

Jonathan Richard[1,2,#], Michael W. Grunst[3,#], Ling Niu[4,#], Marco A. Díaz-Salinas[5,#], Li Zhu[6,#] William D. Tolbert[4], Lorie Marchitto[1,2], Derek Yang[7], Joseph Sodroski[8,9], Amos B. Smith III[7], Priti Kumar[6,*], Walther Mothes[3,*], James B. Munro[5,10,*], Marzena Pazgier[4,*], Andrés Finzi[1,2,11,*]

[1]Centre de Recherche du CHUM, Montréal, Québec, Canada [2]Département de Microbiologie, Infectiologie et Immunologie, Université de Montréal, Montréal, Québec, Canada [3]Department of Microbial Pathogenesis, Yale University School of Medicine, New Haven, CT, USA [4]Infectious Diseases Division, Department of Medicine, Uniformed Services University of the Health Sciences, Bethesda, MD, USA [5] Department of Microbiology, University of Massachusetts Chan Medical School, Worcester, Massachusetts, USA [6] Section of Infectious Diseases, Department of Internal Medicine, Yale University School of Medicine, New Haven, CT, USA [7]Department of Chemistry, School of Arts and Sciences, University of Pennsylvania, Philadelphia, PA, USA [8]Department of Cancer Immunology and Virology, Dana-Farber Cancer Institute, Boston, Massachusetts, USA [9]Department of Microbiology, Harvard Medical School, Boston, Massachusetts, USA [10]Department of Biochemistry and Molecular Biotechnology, University of Massachusetts Chan Medical School, Worcester, MA, USA [11] Lead contact **#** co-first authors ***corresponding authors**

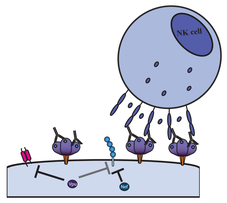
BACKGROUND

Protection from ADCC



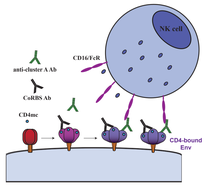
Veillette *et al.*, J.Virol 2014; Veillette *et al.*, J.Virol 2015

ADCC

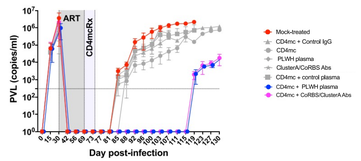


Richard *et al.*, PNAS 2015

A cocktail of anti-CoRBS Abs/anti-Cluster A Abs/CD4mc sensitizes HIV-1-infected cells to ADCC and significantly delays viral rebound after ART interruption in humanized mice

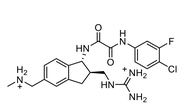


Richard *et al.*, EBioMedicine 2016; Anand *et al.*, JVirol 2019

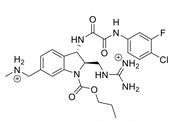


Rajashekar, Richard *et al.*, Cell Host Microbe 2021

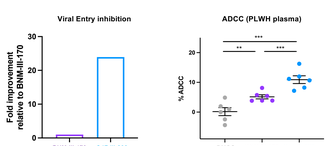
New indoline CD4mcs show improved potency and breath over indane CD4mcs



BNM-III-170 (indane CD4mc)



CJF-III-288 (indoline CD4mc)



Fritschi *et al.*, PNAS 2023

METHODS

- The ability of nnAbs to mediate ADCC with indane or indoline CD4mcs was tested *in vitro* by flow cytometry and their impact on viral rebound was evaluated *in vivo* in HIV-1-infected humanized mice.
- The impact of indoline CD4mc on Env conformation was evaluated by smFRET, cryo-EM and cryo-ET.

RESULTS

Indoline, but not indane or piperidine CD4mc enable anti-CoRBS to mediate ADCC

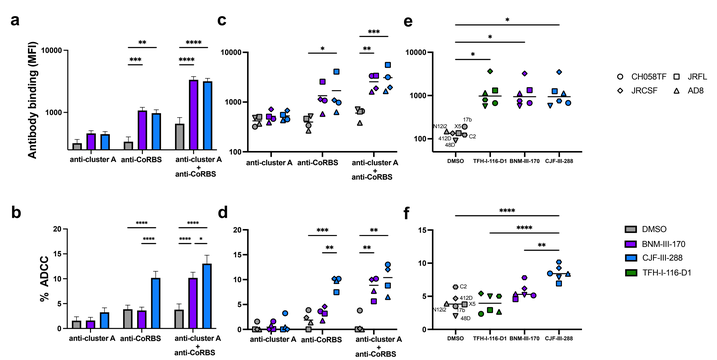


Figure 1. a, Recognition and b, ADCC-mediated elimination of primary CD4+ T cells infected with HIV-$1_{CH058TF}$ by anti-cluster A and anti-CoRBS Abs, alone or in combination, in the presence of 50 µM of indicated CD4mc or equivalent volume of DMSO. c, Recognition and d, ADCC-mediated elimination of primary CD4+ T cells infected with indicated IMCs by anti-cluster A and anti-CoRBS, alone or in combination, in the presence of 50 µM of indicated CD4mc or equivalent volume of DMSO. e, Recognition and f, ADCC-mediated elimination of primary CD4+ T cells infected with HIV-$1_{CH058TF}$ by indicated anti-CoRBS Abs in the presence of 50 µM of indicated CD4mc or DMSO

CJF-III-288 enhances nnAbs binding at concentrations where BNM-III-170 remains ineffective

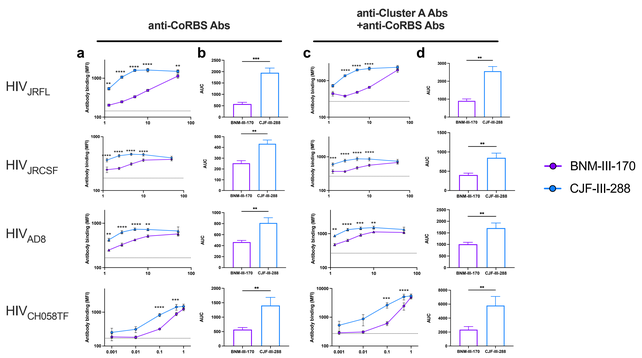


Figure 2 a-d, Recognition of primary CD4+ T cells infected with indicated IMC by anti-CoRBS Ab (17b) alone or in combination with anti-cluster A Ab (A32), in the presence of indicated concentrations of BNM-III-170 or CJF-III-288. a,c, Graphs represent the median fluorescence intensities (MFI) obtained in at least 4 independent experiments with each IMCs . b,d, Graphs represent the area under the curve (AUC) calculated from the MFI obtained in a and c.

CJF-III-288 is more potent than BNM-III-170 in sensitizing HIV-1-infected cells to ADCC

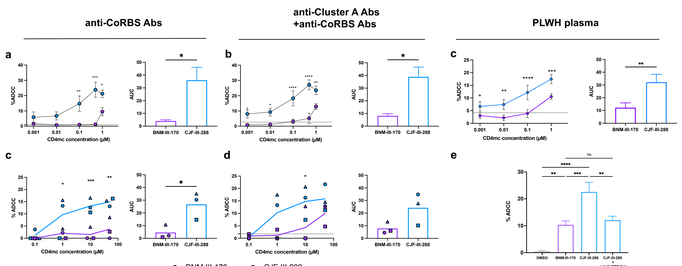


Figure 3. a-c, ADCC-mediated elimination of HIV-$1_{CH058TF}$-infected CD4+ T cells by anti-CoRBS Abs alone or in combination with anti-cluster A Abs or by plasma from PLWH, in the presence of indicated concentrations of BNM-III-170 or CJF-III-288. d-e,ADCC-mediated elimination of *ex-vivo*-expanded CD4+ T cells from three PLWH under ART by anti-CoRBS Abs alone or in combination with anti-cluster A Abs, in the presence of indicated concentrations of BNM-III-170 or CJF-III-288. Left graphs represent the ADCC response obtained at different CD4mc concentrations, while right graphs represent the area under the curve (AUC) of ADCC response. e, ADCC-mediated elimination of HIV-$1_{CH058TF}$-infected primary CD4 T cells preincubated or not with 17b Fab fragments, by plasma from PLWH in the presence of 1 µM of BNM-III-170 or CJF-III-288

Treatment of HIV-1-infected NSG-IL15 humanized mice with an indoline but not an indane CD4mc and a CoRBS Ab delays viral rebound after ART interruption

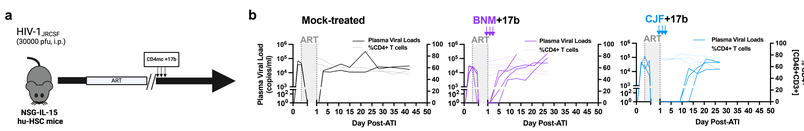


Figure 4. a, Experimental outine. HIV$_{JRCSF}$-infected NSG-IL15 hu-HSC mice were mock treated or treated with indicated CD4mc+17b at ART interruption. b, PVL was measured by real-time qPCR and the % of CD4+ T cells by flow cytometry

CJF-III-288, in combination with anti-CoRBS Abs or PLWH plasma, stabilizes the State-3 Env conformation

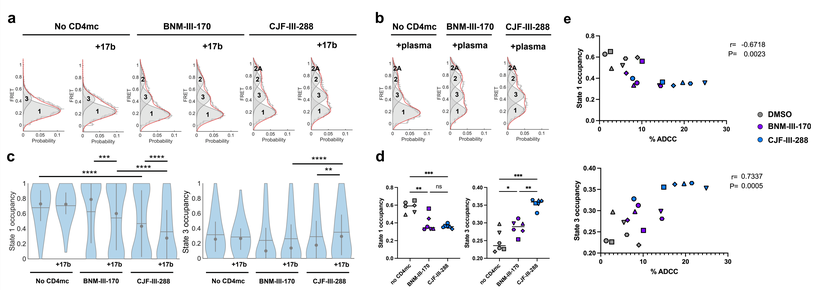
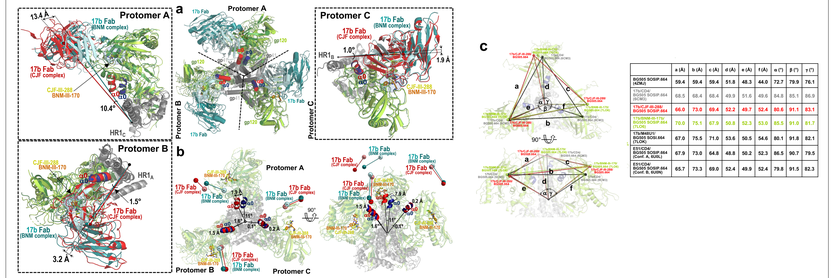


Figure 5. a,b Histograms of FRET values compiled from the population of individual HIV-1_{JRFL} Env trimers on the virion surface in the absence or presence of CD4mc (BNM-III-170 or CJF-III-288), the anti-CoRBS Ab 17b, or PLWH plasma. Histograms are presented as the mean determined from three technical replicates with error bars reflecting the standard error. Overlaid on the histograms are Gaussian distributions determined from HMM analysis of the individual FRET trajectories. Conformational state labels (States 1, 2, 2A, and 3), which have been previously identified are indicated on the corresponding Gaussian. c,d, The occupancies in States 1 and State 3 were calculated from the HMM analysis for each trace and represented with violin plots. e, Correlation between State 1 and State 3 occupancy and ADCC mediated by plasma from PLWH d, e, Each shape represents a different plasma from PLWH.

CJF-III-288 induces an asymmetric opening of Env that modifies the orientation of anti-CoRBS Abs



	a (Å)	b (Å)	c (Å)	α (°)	β (°)	γ (°)
BG505 SOSIP.664 (4ZMJ)	59.4	59.4	58.4	51.8	46.3	44.0
17b/CJF-III-288/ BG505 SOSIP.664 (6MLO)	68.5	68.4	68.4	49.9	51.8	49.6
17b/CJF-III-288/ BG505 SOSIP.664 (7LO6)	66.9	73.0	68.4	52.2	49.7	52.4
17b/BNM-III-170/ BG505 SOSIP.664 (7LO8)	70.0	75.1	67.9	50.8	52.3	53.0
17b/BNM-III-170/ BG505 SOSIP.664 (7LOA)	67.0	75.5	71.0	53.6	50.5	54.6
EPI/CH/ SOSIP.664/ BNM-III-170 (7LO1)	67.9	73.0	64.8	48.8	50.2	52.3
EPI/CH/ BG505 SOSIP.664 (CHIT & RUNG)	65.7	73.3	69.0	52.4	49.9	52.4

Figure 6. a, CJF-III-288-BG505 SOSIP.664-17b Fab and BNM-III-170-BG505 SOSIP.664-17b Fab (PDB:7LO6) complexes superimposed based upon gp120/gp41 protomers. *Center*, the gp120 and gp41 in the CJF-III-288 and BNM-III-170 complexes are shown as ribbons in darker and lighter shades of green/grey, respectively (the α0 helix is shown as red/blue). *Right and left* , blow-up views show the structural alignments of Protomers A, B and C; the 17b Fab is colored light and dark cyan for the BNM-III-170 complex and red for the CJF-III-288 complex. The angle of approach for 17b in each complex is shown by a line drawn from the center of gp41 and the center of mass of the Fab variable domain with the distance between the Fab centers shown above by a black arrow. The relative Fab displacements for each protomer of the two aligned complexes were calculated as angles based upon three points, the centers of two adjacent Fabs and the center of gp41. The center of gp41 was used as the hinge point. b, Changes to the opening of the timer induced by CJF-III-288 or BNM-III-170. The CJF-III-288-BG505 SOSIP.664 and BNM-III-170-BG505 SOSIP.664 trimers are shown superimposed based upon gp120/gp41 protomers (colored as in panel a). Relative bound positions of 17b Fab from each complex are shown with heavy- and light-chain (V_H and V_L) positions determined by the center of mass of their α-carbon atoms (displayed as balls). The distance between the centers of the α0-helices in the two structures in the superimposed trimers is shown above with a black arrow indicating the rotation of the helix. The relative α0-helix displacements for each protomer of the two aligned complexes were calculated as angles based upon three points, the centers of two adjacent α0-helices and the center of gp41. The center of gp41 was used as the hinge point. c, Changes to overall Env trimer assembly, calculated based upon changes to the position of the α-carbon of S375 relative to the gp41 center. Distances between the 375 Cα of each protomer (a, b c), the 375Cα and the gp41 center (d, e, f) and the angle between the gp41 center and two neighboring 375 Cα's (α, β, γ) are shown.

CryoET structure of HIV-1 Env in complex with CJF-III-288 and 17b Abs confirms the asymmetric opening of Env

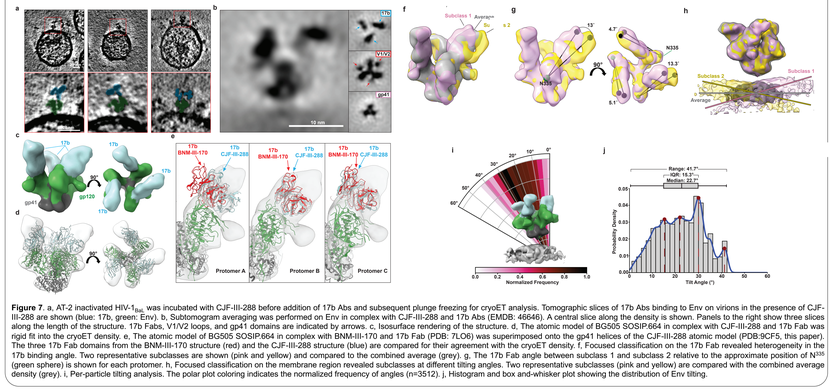
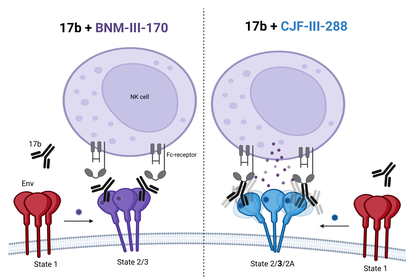


Figure 7. a, AT-2 inactivated HIV-1_{BaL} was incubated with CJF-III-288 before addition of 17b Abs and subsequent plunge freezing for cryoET analysis. Tomographic slices of 17b Abs binding to Env on virions in the presence of CJF-III-288 are shown (blue: 17b, green: Env). b, Subtomogram averaging was performed on Env in complex with CJF-III-288 and 17b Abs (EMDB: 46646). A central slice along the density is shown. Panels to the right show three slices along the length of the structure. 17b Fabs, V1/V2 loops, and gp41 domains are indicated by arrows. c, Isosurface rendering of the structure. d, The atomic model of BG505 SOSIP.664 in complex with CJF-III-288 and 17b Fab was rigid fit into the cryoET density. e, The atomic model of BG505 SOSIP.664 in complex with BNM-III-170 and 17b Fab (PDB: 7LO6) was superimposed onto the gp41 helices of the CJF-III-288 atomic model (PDB:9CF5, this paper). The three 17b Fab domains from the BNM-III-170 structure (red) and the CJF-III-288 structure (blue) are compared for their agreement with the cryoET density. f, Focused classification on the 17b Fab revealed heterogeneity in the 17b binding angle. Two representative subclasses are shown (pink and yellow) and compared to the combined average (grey). g, The 17b Fab angle between subclass 1 and subclass 2 relative to the approximate position of N^{295} (green sphere) is shown for each protomer. h, Focused classification on the membrane region revealed subclasses at different tilting angles. Two representative subclasses (pink and yellow) are compared with the combined average density (grey). i, Per-particle tilting analysis. The polar plot coloring indicates the normalized frequency of angles (n=3512). j, Histogram and box and-whisker plot showing the distribution of Env tilting.

CONCLUSIONS

- **The indoline CD4mc CJF-III-288 enables anti-CoRBS Abs to mediate ADCC**
- **CJF-III-288 exposes the CoRBS and sensitizes infected cells to ADCC by anti-CoRBS Abs or plasma from PLWH, at concentrations where indane CD4mcs fail.**
- **In humanized mice, CJF-III-288 with a CoRBS Ab alone delays viral rebound after ART interruption.**
- **Structural and conformational analyses reveal that CJF-III-288 stabilizes an asymmetric "open" State-3 Env conformation that alters anti-CoRBS Ab orientation.**



➢**CJF-III-288 induces an "open" asymmetric Env conformation modifying the binding orientation of anti-CoRBS Abs, boosting their ADCC activity.**

The views expressed in this presentation are those of the authors and do not reflect the official policy or position of the Uniformed Services University, US Army, the Department of Defense, or the US Government.

NIH National Institutes of Health · INNOVATION.CA CANADA FOUNDATION FOR INNOVATION · FONDATION CANADIENNE POUR L'INNOVATION · Fonds de recherche Santé Québec · CIHR IRSC Canadian Institutes of Health Research / Instituts de recherche en santé du Canada · Canada Research Chairs / Chaires de recherche du Canada · Réseau SIDA-MI · ERASE HIV